

MEASURABLE REALISTIC IMAGE-BASED 3D MAPPING

Wenyang Liu¹, Jinling Wang², Jianguo Jack Wang³, Weidong Ding⁴, Ali Almagbile⁵

^{1, 2, 4, 5} School of Surveying and Spatial Information Systems, University of New South
Wales, Sydney, NSW 2052, Australia;

¹ wenyang.liu@student.unsw.edu.au

³ Faculty of Engineering and Information Technology, University of Technology, Sydney
PO Box 123 Broadway, Ultimo, NSW 2007, Australia

KEY WORDS: Three-dimensional Map, Multi-sensor, Measurable Image, Virtual Reality

ABSTRACT: Maps with 3D visual models are becoming a remarkable feature of 3D map services. High-resolution image data is obtained for the construction of 3D visualized models. The 3D map not only provides the capabilities of 3D measurements and knowledge mining, but also provides the virtual experience of places of interest, such as demonstrated in the Google Earth. Applications of 3D maps are expanding into the areas of architecture, property management, and urban environment monitoring. However, the reconstruction of high quality 3D models is time consuming, and requires robust hardware and powerful software to handle the enormous amount of data. This is especially for automatic implementation of 3D models and the representation of complicated surfaces that still need improvements with the visualisation techniques. The shortcoming of 3D model-based maps is the limitation of detailed coverage since a user can only view and measure objects that are already modelled in the virtual environment.

This paper proposes and demonstrates a 3D map concept that is realistic and image-based, that enables geometric measurements and geo-location services. Additionally, image-based 3D maps provide more detailed information of the real world than 3D model-based maps. The image-based 3D maps use geo-referenced stereo images or panoramic images. The geometric relationships between objects in the images can be resolved from the geometric model of stereo images. The panoramic function makes 3D maps more interactive with users but also creates an interesting immersive circumstance. Actually, unmeasurable image-based 3D maps already exist, such as Google street view, but only provide virtual experiences in terms of photos. The topographic and terrain attributes, such as shapes and heights though are omitted. This paper also discusses the potential for using a low cost land Mobile Mapping System (MMS) to implement realistic image 3D mapping, and evaluates the positioning accuracy that a measurable realistic image-based (MRI) system can produce. The major contribution here is the implementation of measurable images on 3D maps to obtain various measurements from real scenes.

1. INTRODUCTION

Map services have been developed over the years. Most current 2D maps provide only street geometry and have low efficiency and capability for navigation applications. With rapid development of computer vision technology, vision sensors like cameras and laser scanners are being brought into the field to produce 3D maps. Virtual Reality has been applied in geographic applications, such as simulations of terrain and urban areas. The visualized correspondence between real objects and virtual objects on 3D maps increases

the navigational value of 3D maps (Li et al. 2008; Hu et al. 2009). 3D maps representing the world as 3D models have become a remarkable feature of modern mapping services. The image data of high resolution or detailed 3D data of the object can be acquired using laser scanners or digital photo measurements (Otani et al. 2004). They not only provide the capabilities of 3D measurements and geospatial knowledge mining, but also create a sense of virtual environment for the place of interest. Such examples can be seen in the Google Earth.

However, the process of constructing high quality 3D models is time consuming, and requires robust hardware and powerful software to support the enormous amounts of data (Otani et al. 2004). In addition, automatic implementation of 3D models is still a challenging issue. The representation of complicated surfaces still needs improvement with in the visualisation techniques. The shortcoming of 3D model-based maps is the limitation of detailed coverage since user can only view, and measure objects that are already modelled in the virtual environment. Therefore, an alternative 3D mapping concept should be considered to provide 3D measurements and localization with accuracy and visual sense. Measurable realistic images, combined with mobile mapping technologies, have been proposed as an alternative solution for 3D mapping applications.

Madeira et al. (2007) used a low cost Mobile Mapping System (MMS) to measure the 3D distances to objective points on stereo images and obtained their absolute coordinates. The limitation of their approach was that the acquired data from MMS had problems with the data synchronisation. While another limitation, is that the systematic errors are not taken into account in the coordinate computations. A further investigation (Madeira et al. 2009) was done using a software package developed in MATLAB to obtain the absolute and relative coordinates for the objects. The data, acquired from vision/GPS/INS sensors of a MMS, had been synchronized through pulse per second (PPS) signals at millisecond accuracy. This approach achieved centimetre level accuracy with the calculated coordinates of selected feature points. The limitation of this method is that the image matching procedure may result in gross errors/mis-matchings. Consequently, they will certainly have an impact on the calculated coordinates. Li et al. (2008) outlined applications of Digital Measurable Images (DMI) to be implemented in the proposed Digital Earth. DMI could improve the efficiency of main functions in the Digital Earth. DMI represented the street environment and roadside objects with geo-referenced images that users could be easily used in road or pavement monitoring for both measurement and localization purposes. Hu et al. (2008) utilized DMI for geo-information services implemented with a network technology. DMI data has been organised and managed with a unique GPS time tag by geo-coding techniques. While DMI can bridge the gap between navigation network and Point of Interest (POI), the time information of DMI was classified and stored in terms of geo-coding indexes. Such geo-information databases integrated DMI with Digital Elevation Model (DEM), Digital Orthophoto Map (DOM), Digital Line Graphic (DLG) and Digital Raster Graphic (DRG) products allows a user to extract information for various application requirements. Actually, unmeasurable image-based 3D maps are already existed, such as Google street view, but only provide virtual experience. The representation of topographic and terrain attributes, such as shapes and heights are all omitted.

In this paper, we propose and demonstrate a new 3D map concept which is based on measurable realistic images that enables spatial measurements and geo-location services. The concept of such 3D maps will directly use geo-referenced stereo images or panoramic images. The 3D space relationship between the objects in the images could be computed from the geometry model of stereo image pairs. The panoramic function could make 3D maps more interactive with users, and also bring an interesting immersive sense of surroundings. The positioning accuracy of a measurable realistic image-based 3D map will be evaluated. The major contribution here is the implementation of measurable images in 3D maps to obtain various measurements from real scene. We have investigated errors on spatial measurements with indoor environment in terms of absolute position coordinate and relative distance measurement. Other contributions are that we have proposed vertical parallaxes and Dilution of Precision (DOP) values of a geo-referenced image to respectively evaluate positioning accuracy and geometric quality of an image pairs.

In the next section, the concept of measurable realistic image-based 3D mapping is introduced. The methodology of our approach is described in detail in the third section. The fourth section will outline the experimental investigation. The conclusions and future work are discussed in the final section.

2. THE CONCEPT FOR MEASURABLE REALISTIC IMAGE-BASED 3D MAPPING

2.1 Measurable Realistic Image-based 3D Maps

Three dimensional maps can represent the physical world provide near-true experience and realistic sense for a user. Measurable images are at the very core of MRI 3D maps. As rapid development of photogrammetry and computer vision, MRI 3D mapping can be applied with aerial or land-based MMSs. The collected measurable images contain absolute orientation parameters which are related to the epipolar model to build natural human stereo vision and measuring-enabled environment for MRI 3D maps. With the help of plug-in tools and Application Programming Interface (API) together with measurable images, application systems for various purposes could be developed to provide suitable functions based on measurable images, like image browsing, relative measurement, and absolute positioning (Li & Shen 2010). Moreover, multi-data integration of MRI 3D maps could enrich the meaning and value of measurable images, such as online MRI 3D maps, the integration of 3D visualization model and measurable images. Measurable images are collected without the requirement of ground control points to analyze positioning and orientation information of the platform. It effectively improves data processing steps, with no need of additional information. MRI 3D maps could impressively represent the true physical attributes of the real world, where the 2D maps and 3D visualization model cannot demonstrate. Virtual reality could improve the situation of immersive sense of a standard stereo mapping system. In addition, panoramic images have been used in many applications for years. It is meaningful for human acknowledgement and naturally provides a realistic feeling for a user. As an aspect of computer vision, a panoramic image is to translate planar images to a 360 degrees' mosaic image by homograph which is to map relationship

between the perspectives of two images with planar surface through corresponding features (Gledhill et al. 2003).

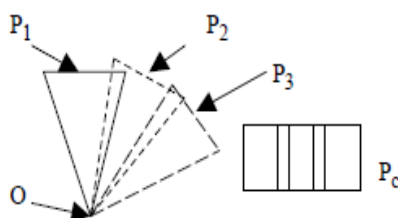


Fig. 1. Panoramic image diagram

Figure 1 shows the capture process of panoramic images with a single camera. Where P_n denotes photos, P_c denotes stitched panoramic image by multiple non-planar image plane, and O is the optical centre of the vision sensor. The adoption of panoramic images will benefit MRI 3D maps significantly in terms of the reduction of both time and costs.

2.2 The Acquisition of Measurable Realistic Images

Measurable realistic images are normally acquired by an MMS that fuses GPS, IMU and vision sensor together to determine the position of objects. Sensors are rigidly mounted on various platforms such as land vehicles and Unmanned Aerial Vehicle (UAV) for the land-based mapping and aerial mapping, respectively. For dynamic surveying, the former sensors determine the position and orientation of the platform. The vision sensors, such as a camera and laser scanner, allow the determination of points external to the platform (Ellum & El-Sheimy 2002). The integration of GPS with IMU improves the reliability of the navigation solution as the inertial sensor errors will accumulate over time. On the contrary, GPS can consistently provide accurate positioning in long periods of time when more than four satellites are visible from the receiver. MMS collects accurate GPS data and angular parameters from the IMU while vision sensors continuously capture realistic images of the surrounding environment. Once realistic images are geo-referenced, photogrammetric parameters can be used to locate the external objects in the mapping coordinate frame. Different from the traditional geo-referencing method, direct geo-referencing method obtains coordinates of objective without ground control points, which need to be surveyed before or after data collection. The quality and reliability of MRI 3D mapping mainly relies on the performance of the multi-sensor system and the system calibration.

The fundamental function model for direct geo-referencing is called a seven-parameter conformal transformation illustrated as below (Ellum & El-Sheimy 2002):

$$\mathbf{r}_p^m = \mathbf{r}_s^m + \boldsymbol{\mu}_s^m \mathbf{R}_s^m \mathbf{r}_p^s \quad (1)$$

Where \mathbf{r}_p^m is the coordinates of a point related to the mapping coordinate frame, it is expressed with seven parameters that the vector \mathbf{r}_s^m with respect to the coordinates of vision sensor in the mapping coordinate frame, \mathbf{r}_p^s indicates to the vector of a point in the

coordinate frame of the vision sensor, μ_s^m and \mathbf{R}_s^m respectively refer to the scale factor and rotation matrix between the vision sensor's coordinate frame and the IMU frame. The scale factor can be derived from stereo image pairs' model, but the rotation matrix between the two coordinate systems usually cannot be directly obtained. When Equation (1) is extended with respect to the position of the GPS receiver and the orientation of IMU, the coordinates of a point relative to time can be expressed as:

$$\mathbf{r}_p^m = \mathbf{r}(t)_{IMU}^m + \mathbf{R}(t)_{IMU}^m (\mathbf{r}_{IMU/s}^{IMU} + \mu_s^{IMU} \mathbf{R}_s^{IMU} \mathbf{r}_p^s) \quad (2)$$

where $\mathbf{r}(t)_{IMU}^m$ is position of IMU in the mapping coordinate frame, $\mathbf{R}(t)_{IMU}^m$ is the rotation matrix between the IMU and mapping coordinate frames, $\mathbf{r}_{IMU/s}^{IMU}$ is the position differences between IMU and vision sensor, normally measured in the system calibration procedures.

3. THE METHODOLOGY FOR MEASURABLE REALISTIC IMAGE-BASED 3D MAPPING

The approach based on a land-based mapping system is to implement and evaluate a MRI 3D map. The basic idea is to build an MRI 3D map that adopted image processing techniques and photogrammetry, respectively. Geo-referenced realistic images or panoramic images, captured from a MMS as described in the previous section, are used to be part of a 3D map. Different from a 3D model map, such new 3D mapping system is easy to operate by users and reduce the mapping costs. The geo-reference data for MRI 3D maps includes stereo images with health overlap between pairs, navigation data and orientation data of image pairs are stored in a database. For positioning and measuring purposes, whenever a user snaps new photos, the images will be matched with the existing images that has already been processed and stored in the database to obtain location information or measurement results. Apart from those basic functions, the proposed system not only utilizing realistic images as a tool for virtual sense, but also employing the measurable realistic images as a spatial sensor for positioning (functioning like GPS). It could benefit indoor navigation services since GPS signals are normally not available indoors.

The most challenging part in photogrammetry and the geo-referencing method is to extract 2D or 3D objects from captured images (Olesk & Wang 2009). It is well understood that image matching is generally classified into a) gray-based matching and b) feature-based matching. As Madeira et al. (2009) commented gray-based matching is based on the use of a point centred template patch in the images in comparing the pixel correlation to another image through along with an epipolar line. The point with the highest correlation is considered to correspondence with the original point. SIFT (Scale-invariant feature transform) is most popular for feature-based matching, as the features have little distortion to image scale and rotation when illumination and image noise are taken into account. It can be used in the proposed system for a reliable image matching solutions, in that a new image is individually matched with the image in the database by comparing SIFT features between new image and the one in the database. The candidate matching features can be found based on the Euclidean distance of their feature vectors (Lowe 2004). The issue of mismatch though of corresponding points, cannot be ignored even with the SIFT algorithm. Figure 2 shows a new image that has been matched with one in the database, but where

there are some obvious mis-matches, e.g., the corner of the left light is matched with the wrong light. The accuracy of positioning and measurement is affected by several factors. First, a camera has inner errors in terms of the lens distortion that includes radial distortion and tangent distortions. Camera calibration is important for data acquisition system to keep the interference of inherent distortions to an acceptable level. On the other hand, the quality of the image matching has an impact on the reliability of MRI 3D maps that relate to the accuracy of the corresponding points in the stereo images. Last factor is the quality of the six degrees of freedom (6DoF) that is essentially influenced by the stereo model geometry.

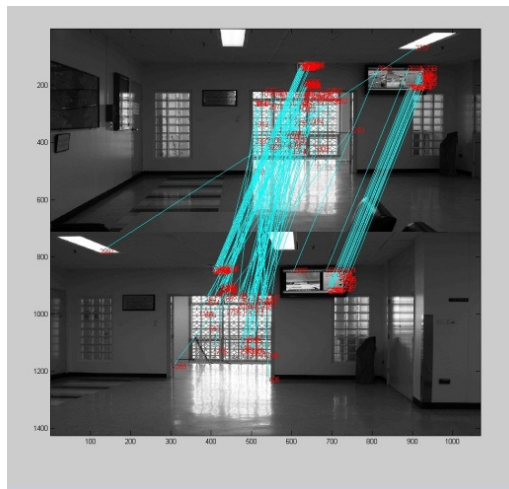


Fig. 2. Illustration of SIFT mismatches for two images

3.1 Position Determination and 6DoF Estimation

Relative orientation with coplanarity constraint based on epipolar geometry is to translate and rotate one image to the stereo partner in the object coordinate frame (Figure 3). The objective coordinates can be resolved from the image coordinate frame (Figure 3) by the relative orientation of the stereo image pairs. The theory is based on the condition that the object point and the vector between two perspective centres of the camera should lie on the same plane.

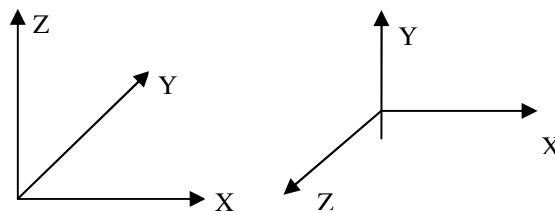


Fig. 3. Object coordinate frame (Left) and image coordinate frame with viewing direction in negative of Z axis (Right)

However, the orientations that usually contain residuals that will result in the rays intersecting to the objective point from two cameras that lie on different planes. This phenomenon is known as y-parallaxes or vertical parallaxes in the stereo case. Vertical parallax is one of many factors expressing the relationship between the image and model coordinates (Luhmann et al. 2006). Cramer & Stallmann (2001) also mentioned this issue, but refer to it as y-parallax. Here we used the term vertical parallax to describe the phenomenon. This is demonstrated in Figure 4 where pY denotes the vertical parallax:

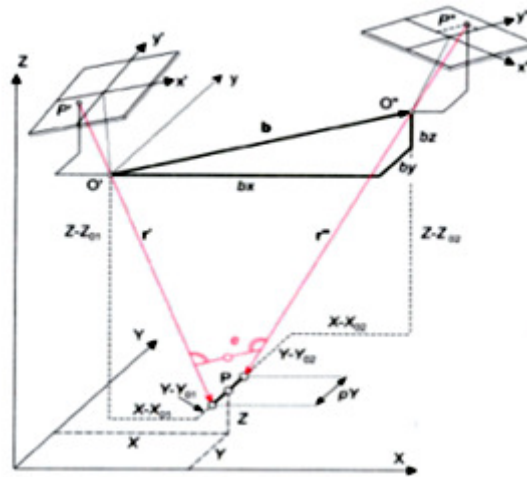


Fig. 4. Vertical parallaxes

6DoF are provided by a data collecting system that includes position elements X, Y, Z and attitudes ω , φ , κ of the vision sensor in the photogrammetric terminology. In an effort to improve the 6DoF accuracy and reliability, a least squares adjustment is used to process the measurements. The functional and stochastic models of the least squares procedures are given by:

$$\mathbf{v} = \mathbf{A}\hat{\mathbf{x}} - \mathbf{l} \quad (3)$$

$$\mathbf{D} = \sigma_0^2 \mathbf{Q} = \sigma_0^2 \mathbf{P}^{-1} \quad (4)$$

$$\hat{\sigma}_0 = \sqrt{\frac{\mathbf{v}^T \mathbf{P} \mathbf{v}}{n-u}} \quad (5)$$

The quality of the 6DoF is vital for coordinate calculations. 6DoF can be obtained in a direct way or indirect way. Regarding the latter method the control points are used to estimate the position and pose of the camera based on collinearity equations:

$$x = x_0 + f \frac{a_1(X-X_0) + b_1(Y-Y_0) + c_1(Z-Z_0)}{a_2(X-X_0) + b_2(Y-Y_0) + c_2(Z-Z_0)} + \Delta x \quad (6)$$

$$y = y_0 + f \frac{a_2(X-X_0) + b_2(Y-Y_0) + c_2(Z-Z_0)}{a_3(X-X_0) + b_3(Y-Y_0) + c_3(Z-Z_0)} + \Delta y \quad (7)$$

The Dilution of Precision (DOP) values can be defined with respect to the impact of geometry changes on the 6DoF through least squares estimation as (Xun et al. 2010):

$$XDOP = G_x \quad YDOP = G_y \quad ZDOP = G_z \quad (8)$$

$$PDOP = \sqrt{G_x^2 + G_y^2 + G_z^2} \quad (9)$$

$$\omega DOP = G_\omega \quad \varphi DOP = G_\varphi \quad \kappa DOP = G_\kappa \quad (10)$$

$$ADOP = \sqrt{G_\omega^2 + G_\varphi^2 + G_\kappa^2} \quad (11)$$

The elements of $G_x, G_\omega \dots$ are derived from the diagonal elements of the matrix $(A^T A)^{-1}$, where A is the design matrix of least squares. The PDOP and ADOP represent the position DOP and attitude DOP, respectively.

4. EXPERIMENTS AND RESULTS

The experiments were conducted in two circumstances including an indoor environment and an outdoor environment. The aim is to evaluate the performance of MRI 3D mapping in both scenarios.

For the indoor case, a calibrated Canon EOS450D camera was used. Its image resolution was high with each image containing 4272*2848 square pixels. The focus length of the camera was 24.7 mm. In order to obtain 6DoF, some control points were pre-surveyed in the local coordinate system by a total station. The origin of the local coordinate frame was the centre of the total station projecting on the ground. The total station also surveyed some points localized on the measurable images whose coordinates were treated as ground truth. Two major investigations were designed. The first investigation was where the distances (calculated with the computed coordinates) from objective points to the total station were compared with the slope distances, measured by the total station. The second investigation concerned the accuracy the absolute coordinates measured.

For the outdoor case, the 6DoF were collected using an integrated multi-sensor platform (Figure 5).



Fig. 5. Multi-sensors mounted on the vehicle

The vision sensor is SONY colour video camera with the resolution of 1024*768 and a sampling rate of approximately 7.5Hz. The positioning sensor is the NovAtel OEM4 GPS receiver. The pseudorange-based DGPS solutions were loosely integrated with Xsens MTI IMU which provides the attitudes of the camera. The sampling rates of the GPS receiver and the IMU sensor were 20 Hz and 100 Hz, respectively. The accuracy of DGPS position is at the 1 meter level and the IMU sensor has an accuracy of 1 degree (RMS) for roll and pitch, and 3 degrees (RMS) for yaw in the dynamic situation. The time resolution is 1 μ s which enables synchronisation accuracy at the 1 ms level. The relative position (lever arm) between the sensors was measured during the system calibration. The test was conducted in a typical urban environment and it lasted for about 5 minutes. The purpose of this road test was to evaluate the quality of various data from a low cost integrated multi-sensor platform using measurable images.

4.1 Indoor Test

The indoor test was carried out in the School's lobby. Two cameras captured stereo images for use in the object positioning. To assess the quality of 6DoF and the accuracy of the MRI 3D map, the indoor experiment used two sets of 6DoF which were relatively obtained by 9 control points and 18 control points. Then 18 points were measured in the overlap area of the collected stereo images (Figure 6).

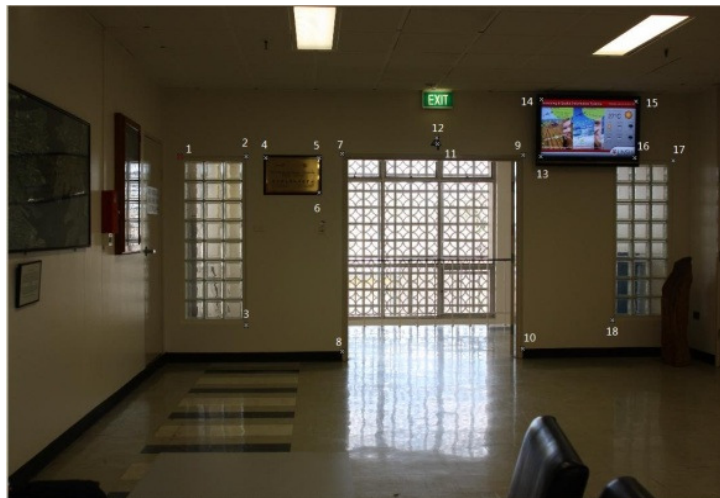


Fig. 6. The 18 measured points by measurable images

Table 1 revealed the errors in the absolute coordinates of the 18 measured points with respect to the solutions based on the 9 control points, while Table 2 illustrated the results from the 18 control point solutions.

Tab. 1. Absolute coordinates with the 9 control points

Points	X error (m)	Y error (m)	Z error (m)	Object distance (m)
1	0.004	0.013	-0.005	7.568
2	0.001	0.006	0.004	7.213
3	0.002	0.008	0.001	6.913
4	-0.004	0.008	-0.003	7.093
5	-0.005	-0.009	-0.006	6.846
6	-0.006	-0.004	0.001	6.749
7	-0.006	-0.001	0.003	6.775
8	-0.004	0.012	-0.004	6.443
9	0.005	-0.003	0.005	6.304
10	0.003	-0.019	-0.003	5.944
11	0.002	-0.012	0.002	6.503
12	0.012	-0.015	0.003	6.529
13	0.006	0.008	0.003	6.150
14	0.006	0.005	-0.001	6.338
15	0.009	0.009	-0.005	6.339
16	0.005	0.021	0.002	6.152
17	-0.012	-0.014	-0.004	6.348
18	0.085	0.035	0.002	5.933
Mean	0.002	0.0050	-0.0007	
RMS	0.008	0.014	0.003	

Tab. 2. Absolute coordinates with the 18 control points

Points	X error (m)	Y error (m)	Z error (m)	Object distance (m)
1	0.008	0.005	0.004	7.568
2	0.003	-0.001	0.003	7.213
3	0.001	0.005	0.002	6.913
4	-0.003	0.002	-0.003	7.093
5	-0.005	-0.010	-0.001	6.846
6	-0.006	-0.005	0.001	6.749
7	-0.006	-0.005	0.003	6.775
8	-0.005	0.003	-0.004	6.443
9	0.006	-0.005	0.005	6.304
10	0.004	-0.004	-0.003	5.944
11	0.001	-0.015	0.001	6.503
12	0.003	-0.015	0.003	6.529
13	0.026	0.005	0.004	6.150
14	0.005	0.006	0.001	6.338
15	0.002	0.012	-0.003	6.339
16	0.002	0.017	0.002	6.152
17	-0.008	-0.017	-0.004	6.348
18	0.002	0.014	0.001	5.933
Mean	0.0017	-0.0004	0.0006	
RMS	0.007	0.010	0.002	

The results show that the accuracy of the computed coordinates for an object is at the millimetre level. Comparing the two sets of results, the mean error and the root mean square of X, Y, and Z in the 9 control point case were slightly higher than those in the 18 control point case. Additionally, the mean of the Z errors in Table 1 and the Y errors in Table 2 were negative which may indicate the existence of some systemic errors. Some errors from image matching and mapping sensor were not detected in this experiment. The

largest errors in the X, Y, and Z directions in both cases were 8.5 cm, 3.5 cm, and 6 mm (Table 1) and 2.6 cm, 1.7 cm, and 5 mm (Table 2) respectively.

The distance measurements are illustrated in Figures 7 and 8. The measured distances in the 9 control point case revealed that the majority of the errors were less than 2 centimetres (Figure 7). The results in the 18 control point case demonstrated that the errors for the most measured points were less than 1 centimetres (Figure 8). Furthermore, the largest error of the former experiment was approximate 3.5 centimetres for point 18, which was located at the low left corner of glass window on the right hand side. For the latter experiment, the largest error was 2 cm, for point 17, which was on the upper right corner of the same window. The ranges between the total station and the 18 object points were from 5.9 m to 7.5 m. Thus centimetre level accuracy can be achieved for these short distances.

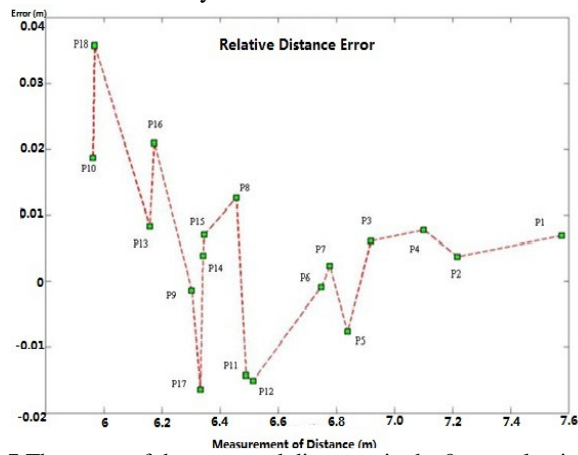


Fig. 7. The errors of the measured distances in the 9 control point case

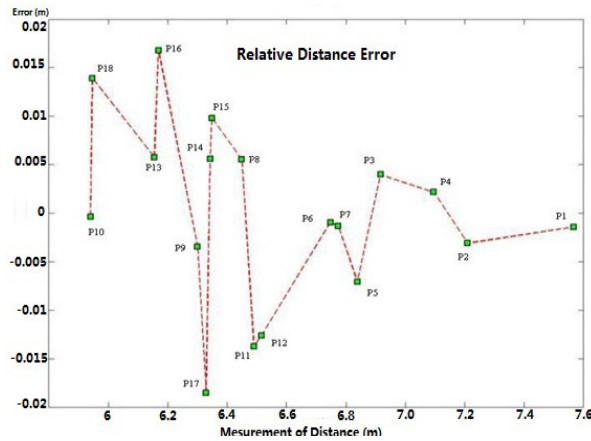


Fig. 8. The errors of the measured distances in the 18 control point case

The vertical parallax can partially illustrate the accuracy of the 6DoF used. The statistics for the two sets of vertical parallaxes are shown in Table 3:

Tab. 3. Vertical parallaxes for the 9 control point case

Points	Point 1	Point 2	Point 3	Point 4	Point 5	Point 6
Vertical parallaxes (m)	0.0001	-0.003	-0.008	-0.002	0.001	-0.002
Points	Point 7	Point 8	Point 9	Point 10	Point 11	Point 12
Vertical parallaxes (m)	-0.001	-0.002	0.001	-0.001	-0.001	0.001
Points	Point 13	Point 14	Point 15	Point 16	Point 17	Point 18
Vertical parallaxes (m)	0.001	0.002	0.004	0.0001	0.002	-0.003

With regard to the results, point 3 had the largest vertical parallaxes in both data sets which were 8 millimetres and 5 millimetres, respectively. The errors for the other points were around 1 millimetre.

The DOP values of the 6DoF were also assessed. The stereo model requires two or more images. In this investigation, two images were used for positioning and the 6DoF of each image was analysed by the DOPs. In the 9 control point case, the PDOP and ADOP of the left image were 6828 and 794.

Tab. 4. Vertical parallaxes in the 18 control point case

Points	Point 1	Point 2	Point 3	Point 4	Point 5	Point 6
Vertical parallaxes (m)	0.002	-0.001	-0.005	-0.0001	0.003	0.001
Points	Point 7	Point 8	Point 9	Point 10	Point 11	Point 12
Vertical parallaxes (m)	-0.0004	-0.001	0.0001	-0.001	-0.001	0.001
Points	Point 13	Point 14	Point 15	Point 16	Point 17	Point 18
Vertical parallaxes (m)	0.002	0.001	0.002	0.001	0.001	-0.003

The right image had slight differences on the PDOP and ADOP, which were 6726 and 788, respectively. For the 18 control point case, the PDOP and ADOP of the left image were 4072 and 558, while the values for the right image were 4036 and 474. The results validated that more control points that can be provided the stronger geomatic model, which improves the precision of the estimated 6DoF.

4.2 Road Test

For the investigation in the outdoor environment, the 6DoF were directly acquired by coupling the low cost sensors. Comparing the data set with the indoor test, the quality of data could not reach millimeter level, but for such a low cost dynamic surveying system, achieving meter level with vertical parallaxes is acceptable. The whole data set contained more than 1000 images. This investigation utilized two images that consisted of a stereo

case for object position determination. 18 points were measured in the measurable images in Figure 9. Most of points were traffic signs, and items on the pavement. The distances between these points ranged from 8m to 30 m. The vertical parallaxes, in Table 5 varied from 0.024 m to 0.892 m. Most of the parallaxes were between 20 centimeters and 30 centimeters, and the largest error was at point 13 which was at the bottom of the right street light. This could be due to some unidentified systematic errors that will be investigated in future studies.



Fig. 9. Measured 18 points on the measurable images selected from the road test.

Tab. 5. Vertical parallaxes for the 18 selected points

Points	Point 1	Point 2	Point 3	Point 4	Point 5	Point 6
Vertical parallaxes (m)	-0.274	-0.081	-0.308	-0.369	-0.220	-0.263
Points	Point 7	Point 8	Point 9	Point 10	Point 11	Point 12
Vertical parallaxes (m)	-0.158	-0.120	-0.238	-0.512	-0.261	0.244
Points	Point 13	Point 14	Point 15	Point 16	Point 17	Point 18
Vertical parallaxes (m)	0.892	0.213	-0.078	0.396	-0.024	-0.120

5. CONCLUSIONS

This paper has introduced the concept of MRI 3D mapping with a multi-sensor integrated platform. The paper has presented a feasible approach of using geo-referenced images as a sensor for object positioning and 3D space measurements. The MRI 3D mapping could be utilized for various applications, such as pavement monitoring, navigation, rescue, and so on. It is also effective in rendering 3D data to 2D data. The currently used measurable image-based system is a prototype system. Thus, the performance of data acquisition can be potentially improved. Future research will focus on the construction of a measurable image database, and the error analysis for a reliable 3D mapping system with low cost sensors.

REFERENCES

- Cramer, M. & Stallmann, D., 2001. On the Use of GPS/Inertial Exterior Orientation Parameters in Airborne Photogrammetry, *Proceedings of the OEEPE Workshop, Integrated Sensor Orientation, Hanover, Germany, 17–18 September*.
- Ellum, C. & El-Sheimy, N., 2002. Land-based Mobile Mapping Systems. *Photogrammetric Engineering and Remote Sensing*, vol.68, no.1, pp.13–17.
- Gledhill, D., Tian, G.Y., Talor, D. & Clarke, D., 2003. Panoramic Imaging--A Review. *Computers & Graphics*, vol. 27, no. 3, pp. 435-445.
- Hu, Q., Liu, S. & Mao, K., 2009. A “Reality Vision” Navigation Technique Based on Sequence Geo Referenced Image Databases, *Critical Issues in Transportation Systems Planning, Development and Management*, ASCE.
- Hu, Q. & Wang, H., 2008. A New Web-based Geo-information Service Approach With Digital Measurable Image Toward Direct Virtual Reality. *ISPRS Congress Beijing 2008*, Commission IV, WG IV/5.
- Luhmann, T., Robson, S., Kyle, S. & Harley, I., 2006. *Close range Photogrammetry: Principles, Techniques and Applications*, Whittles, United Kingdom.
- Li, D., Huang, J. & Shao, Z., 2008. Digital Earth with Digital Measurable Images. *The International Archives of the Photogrammetry, Remote Sensing and Spatial Information Sciences*. vol. XXXVII, part no. B4.
- Li, D. & Shen, X., 2009. Geospatial Information Service Based on Digital Measurable Image. *Geo-Spatial Information Science*, vol. 13, no. 2, pp. 79-84.
- Li, D., Wang, M. & Gong, J., 2002. Principle and Implement of Measurable Virtual Reality (MVR) Based on Seamless Stereo-orthoimage Database. *The International Archives of the Photogrammetry, Remote Sensing and Spatial Information Sciences*. vol. XXX IV, part no. 5/W3.
- Li, X., Wang, J., Olesk, A., Knight, N. & Ding, W., 2010. Indoor Positioning within a Single Camera and 3D Maps. *Ubiquitous Positioning Indoor Navigation and Location Based Service (UPINLBS)*, Helsinki, Finland.
- Lowe, D.G., 2004. Distinctive Image Features from Scale-invariant Keypoints. *International Journal of Computer Vision*, vol.60, no.2, pp.91-110.
- Madeira, S., Gonçalves J. & Bastos, L., 2007. Implementation of A Low Cost Mobile Mapping System. *5th International Symposium on Mobile Mapping Technology*, Padua, Italy.
- Madeira, S., Gonçalves, J. & Bastos, L., 2010. Photogrammetric Mapping and Measuring Application Using MATLAB. *Computers & Geosciences*, vol.36, no.6, pp.699-706.
- Olesk, A., & Wang, J., 2009. Geometric and Error Analysis for 3D Map-matching. *International Global Navigation Satellite Systems Society, IGNSS Symposium 2009*, Australia.
- Otani, H., Aoki, H., Ito, T. & Kochi, N., 2004. 3D Model Measuring System. *The International Archives of Photogrammetry and Remote Sensing*, Commission V, WG V/2.